data

MDPI

Article

Data-Driven Analysis of MRI Scans: Exploring Brain Structure Variations in Colombian Adolescent Offenders

Germán Sánchez-Torres [1], Nallig Leal [2] and Mariana Pino [3,*]

[1] Facultad de Ingeniería, Universidad del Magdalena, Santa Marta 470004, Colombia; gsanchez@unimagdalena.edu.co
[2] Facultad de Ingenierías, Universidad Autónoma del Caribe, Barranquilla 080001, Colombia; nleal@uac.edu.co
[3] Programa de Psicología, Universidad Autónoma del Caribe, Barranquilla 080020, Colombia
* Correspondence: mariana.pino@gmail.com

Abstract: With the advancements in neuroimaging techniques, understanding the relationship between brain morphology and behavioral tendencies such as criminal behavior has garnered interest. This research addresses the investigation of disparities in neuroanatomical structures between adolescent offenders and non-offenders and considers the implications of such distinctions regarding offender behavior within adolescent populations. Employing data-driven methodologies, MRI scans of adolescents from Barranquilla, Colombia, were analyzed to explore morphological variations. Utilizing a 1.5 Tesla Siemens resonator (Siemens Healthineers, Erlangen, Germany), T1-weighted MPRAGE anatomical images were acquired and analyzed using a systematic five-step methodology including data acquisition, MRI pre-processing, feature selection, model selection, and model validation and evaluation. Participants, both offenders and non-offenders, were aged 14–18 and selected based on education, criminal history, and physical conditions. The research identified significant disparities in the volumes of 42 brain structures between adolescent offenders (AOs) and non-offenders (NOs), highlighting particular brain regions potentially associated with offending behavior. Additionally, a considerable proportion of AOs emanated from lower socioeconomic backgrounds and showcased marked substance use. The findings suggest that neuroanatomical disparities potentially correlate with criminal behavior among adolescents at a neurobiological level. Noticeable socio-environmental factors, such as lower socioeconomic status and substance abuse, were substantially prevalent among AOs. Particularly, neurobiological deviations in structures like ctx-lh-rostralmiddlefrontal and ctx-lh-caudalanteriorcingulate perhaps represent a link between neurological factors and external stimuli.

Keywords: magnetic resonance imaging; adolescent offenders; emotional regulation; criminal behavior

Citation: Sánchez-Torres, G.; Leal, N.; Pino, M. Data-Driven Analysis of MRI Scans: Exploring Brain Structure Variations in Colombian Adolescent Offenders. *Data* **2024**, *9*, 7. https://doi.org/10.3390/data9010007

Academic Editor: Alain Lalande

Received: 2 September 2023
Revised: 18 December 2023
Accepted: 22 December 2023
Published: 26 December 2023

1. Introduction

Data-driven methodologies are helping fields from healthcare to neuroscience, enhancing understanding and outcomes [1]. In neuroscience, advanced imaging techniques are deepening the understanding of the relationship between the brain and criminal tendencies. Professionals in law enforcement and mental health have long studied the relationship between the human brain and criminal behavior [2–5]. It is widely accepted that both genetics and environment significantly shape a juvenile's inclination towards delinquent conduct during their developmental stage [6–10]. These traditional understandings have been foundational, yet recent advancements in neuroimaging techniques have ushered in an additional perspective, suggesting that variations in cerebral anatomy and physiology might also play a pivotal role [11,12].

The existing literature has examined behavioral and cognitive differences between adolescent offenders (AOs) and non-offenders (NOs) [13–18]. Emotional regulation (ER) and its dysfunction (ERD) are central themes, with ERD being consistently linked to

behavioral challenges and juvenile delinquency [19–23]. Furthermore, links between ERD and other forms of delinquency, such as minor rule-breaking and substance abuse, have been observed [24–27]. Another significant correlation lies between ER and aggression; individuals with ERD often exhibit more aggressive tendencies than their counterparts without ERD [27,28]. Despite these documented associations, the relationship between ER and delinquency appears to be more intricate than initially believed.

Recent advancements in magnetic resonance imaging (MRI) have enriched this address [28]. MRI provides a non-invasive, high-quality examination of brain structures, allowing researchers to explore neuroanatomical variations and potential associations with behavioral traits. Some studies have leveraged MRI to investigate correlations between cortical thickness and criminal conduct [29–31]. For instance, certain regions of the brain associated with decision-making, impulse control, and moral reasoning were found to have diminished gray matter volume in various regions such as the right superior frontal gyrus, right middle and superior temporal regions, and left inferior parietal lobe, in young offenders [3]. Similarly, structural and functional impairments in regions linked to antisocial tendencies were identified [32].

However, despite these findings, research exploring neuroanatomical correlations, especially concerning the volume of brain structures, is still of interest to the academic community. This presents a significant research gap, signaling the need for more in-depth investigations.

This study seeks to delve deeper into the neuroanatomical differences between juvenile delinquents and individuals who have not engaged in criminal activities. Utilizing MRI scans from both groups, the primary objective is to identify statistically significant differences in segmented brain structures and pinpoint key structures that might be instrumental in distinguishing between the two groups.

Understanding these neuroanatomical variations is not just about validation; it paves the way for enhancing our grasp of the computational methods used in characterizing brain anatomy. Such insights can potentially refine risk assessment tools and interventions by identifying specific brain structures associated with criminal behavior.

The subsequent sections of this article are organized in a methodical fashion to provide a comprehensive understanding of our research. Section 2 encompasses a comprehensive literature review, wherein we meticulously analyze previous research and pertinent discoveries related to our selected topic. This statement provided a foundational framework and context for our respective scholarly investigations. Section 3 presents a detailed description of the materials and methods we employed in the study, including an explanation of the experimental design, data collection methods, and analytical approaches utilized. Section 4 presents the findings of our study. In Section 5, we conduct a thorough analysis in which we interpret our results, compare them with existing scholarly works, and draw conclusions based on the evidence at hand.

2. Materials and Methods

The methodology was developed through a systematic sequence of steps (see Figure 1), with a particular emphasis on obtaining MRI scans from the subjects involved in the investigation. The MRI scans were subjected to a comprehensive preprocessing stage to eliminate any possible potential confounding factors. The preprocessing stage involved a three-tiered approach that encompassed several steps, namely motion correction, conformation, intensity normalization, skull stripping, volumetric registration, and tissue segmentation.

The process of selecting features was carried out through statistical and machine learning approaches. A statistical hypothesis test was used in order to facilitate the identification of significant features from a statistical perspective. Machine learning techniques like Recursive Feature Elimination (RFE) [33] and Least Absolute Shrinkage and Selection Operator (LASSO) [34] methodologies were used to increase the potential classification capabilities.

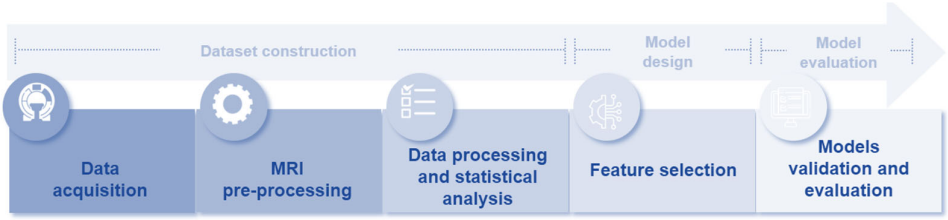

Figure 1. General methodology of the study.

The final phase encompassed the selection of classification methods, evaluating the performance of the classification models, and considering metrics like precision, recall, F1-score, and model accuracy.

2.1. Data Acquisition

2.1.1. Participants

This research involved a group of teenage individuals who had committed offenses (Adolescent offenders—AOs) and another group of teenage individuals who had not (non-offenders—NOs), all aged between 14 and 18 and identifying as male. The groups consist of 66 individuals for the NOs (non-offenders) and 65 individuals for the AOs (adolescent offenders), respectively. The offenders were selected from Fundación Clarets, Centro de Reeducación el Oasis y Fundación Luz Esperanza in Barranquilla, Colombia, where they were incarcerated for crimes such as sexual abuse, homicide, and theft. The non-offenders were chosen from various educational institutions in the same city, and they had to meet specific criteria: being male, aged 14 to 18, having no more than 12 years of education, lacking a criminal history, and not having any neurological, psychiatric, or physical conditions.

2.1.2. Ethics Statement

Both groups obtained informed consent from their parents or legal guardians, either voluntarily or, in the case of participants under 18, with parental or guardian consent. The study received approval from the Universidad del Magdalena Ethics Committee and adhered to the ethical principles outlined in the Declaration of Helsinki.

2.1.3. Instruments

The magnetic resonance imaging (MRI) scans were obtained utilizing a 1.5 Tesla Siemens resonator that was equipped with a 32-channel head coil. The acquisition of T1-weighted anatomical images was carried out through the utilization of a Magnetization Prepared Rapid Gradient Echo (MPRAGE) sequence, which involved the use of single-shot echoplanar images. The imaging parameters used were TR/TE of 10/4.6 ms, voxel size of 1 mm $\times$ 1 mm $\times$ 1 mm, gap between slices of 0.1 mm, matrix size of 160 $\times$ 256 $\times$ 256, and a total of 160 slices. The study employed a field of view (FOV) of 250 mm along the read direction, with a phase FOV of 100%. The imaging system utilized a base resolution of 256, accompanied by a phase resolution of 100% and slice resolution of 83%, resulting in a slice thickness of 1 mm.

The experiments were conducted on a computer equipped with an Intel Xeon Gold 6230R 2.10G 2933 MHz 52-core processor (Intel, Santa Clara, CA, USA), 256 GB DDR4 2933 memory, and 2 NVIDIA RTX A6000 48 GB DH (NVIDIA, Santa Clara, CA, USA).

2.2. MRI Preprocessing

The preprocessing stage of MRI image analysis has been partitioned into three distinct phases, with the aim of optimizing the performance of the Freesurfer software tool version 7.4.1 [35] in a manner that is both efficient and streamlined. The aforementioned stages were executed individually to mitigate the risk of data loss or operational disruptions.

Phase 1: The primary procedure involves rectifying any motion artifacts that may have occurred during the scanning process and subsequently aligning the image to ensure uniformity in voxel dimensions and image size. Subsequently, the Non-Uniform Intensity Normalization (NU) [36,37] technique is employed to account for the MRI image intensity fluctuations that frequently arise from irregularities in the RF field. The process of Talairach transform computation is utilized to align the MRI image to the standard anatomical Talairach space [38]. Following this, the initial stage of intensity normalization is executed to improve the uniformity of tissue intensity. The final step in this phase entails the elimination of extraneous tissue, predominantly the cranium and integument, from the MRI scan through a technique referred to as skull stripping. An additional step has been incorporated to compute the estimation of intracranial volume.

Phase 2: Encompasses the utilization of Expectation-Maximization (EM) Register [39] and a linear volumetric registration technique, succeeded by controlled averaging (CA) intensity normalization. Subsequently, the CA Non-linear Volumetric Registration technique is executed, and then the image's neck region is eliminated. A following iteration of the EM Register procedure has been executed, wherein the image now incorporates the skull. The proposed methodology involves a CA Label operation for volumetric labeling and statistical analysis, followed by an additional round of intensity normalization, white matter segmentation, and removal of the white matter region. After, this phase is concluded by a series of procedures comprising Fill, Tessellation, Smooth1, Inflate1, QSphere, Automatic Topology Fixer, Final Surfs, Smooth2, and Inflate2.

Phase 3: Commences with Spherical Mapping and Spherical Registration, encompassing the Contralateral hemisphere. Later, the mean curvature is assigned to the participant and successively subjected to the Cortical Parcellation procedure, which entails the utilization of the Desikan_Killiany and Christophe Labeling techniques. Consequently, statistical computations are performed on the cortical parcellation data, followed by the application of a cortical ribbon mask, and finally, the mapping of cortical parcellation to Aseg is executed.

2.3. Data Processing and Statistical Analysis

2.3.1. Demographic Description

Including age and gender, data were gathered for participants in both the AO and NO groups. Descriptive statistics such as mean, standard deviation, and range were used to characterize their age distribution. Moreover, the distribution of participants across distinct socioeconomic levels was recorded to identify potential correlations between socioeconomic status and offender behavior. Additionally, data on the consumption of various substances, including SPA, alcohol, marijuana, and cocaine, were collected, allowing for the differentiation of substance intake patterns between the offender and non-offender groups.

2.3.2. Brain Structural Analysis

For the analysis of brain structure, two-sample *t*-tests were conducted to evaluate the sociodemographic and clinical attributes of the participants. Given the violations of normality and homoscedasticity assumptions, the Mann–Whitney test was chosen for the further analysis of brain structures. A threshold of $p < 0.05$ was set to determine statistical significance. In addition, effect size was quantified using Cohen's d. Concurrently, an analysis was designed to compare variations in the volumes of brain structures across different age groups for both the AOs and NOs cohorts. The intent was to discern any consistent patterns or trends related to age in the volume of specific brain structures.

2.4. Feature Selection and Model Evaluation

A wide-ranging methodology was employed to distinguish the significant characteristics that differentiate the AO group from the NO group. This approach involved the integration of statistical analyses and machine learning algorithms. The main objective was to ascertain the variables that exhibit statistically significant differences among the individuals belonging to the two groups.

The feature selection process began with an initial stage that involved the utilization of statistical hypothesis testing to assess the individual significance of each feature. This facilitated the discernment of variables that exhibited significant divergence between the two groups. It was hypothesized that characteristics exhibiting statistical significance below a pre-established threshold (e.g., $p < 0.05$) could have pertinent prognostic capabilities and, therefore, they were chosen for additional investigation.

Principal component analysis (PCA) was later employed as a technique for reducing dimensionality. PCA is a statistical technique that aims to extract the principal components from a dataset in order to capture the highest possible amount of variance while using the minimum number of components. The outcome of this conversion yielded a new group of perpendicular variables that were derived from linear combinations of the initial characteristics. This facilitated the mitigation of probable overfitting caused by the ill effects of the number of dimensions. The inclusion of PCA was strictly to assess the possibility of significant reduction and to indicate that a substantial portion of the dataset's variability could be explained with a reduced number of features.

During the last stage of the feature selection procedure, advanced machine learning methodologies such as Recursive Feature Elimination (RFE) and Least Absolute Shrinkage and Selection Operator (LASSO) were utilized. The RFE approach functions through a process of successive feature elimination and an evaluation of the model's efficacy, with the aim of identifying the subset of features that exert the greatest influence on the prediction. In contrast, LASSO works as a regularization technique that can augment the predictive precision and interpretability of the statistical model to which it is applied. This is achieved by compelling the coefficients of less significant features to assume a value of zero, thereby executing feature selection.

This structured design of methodology allows us to ensure a comprehensive and methodical selection of features, thereby optimizing the potential for identifying the key variables that distinguish the AO and NO groups.

3. Results

3.1. Participants

The AO group consisted of 65 youth offenders, all of whom were male. The age distribution of the study group was characterized by a mean (M) age of 16.9 years, a standard deviation (SD) of ±0.97 years, and an age range (R) spanning 15 to 18 years. The NOs consisted of 66 youth offenders, all of whom were male. The age distribution of this group was characterized by a mean age (M) of 16.36 years, a standard deviation (SD) of ±1.10 years, and an age range (R) spanning 14 to 18 years (see Figure 2).

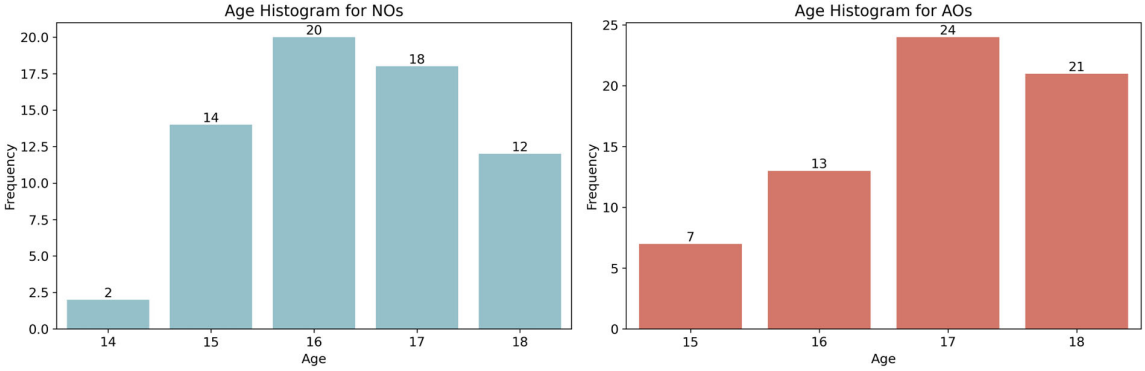

Figure 2. Age distribution histograms for control and study groups.

Table 1 shows some descriptive statistics into the age distributions and central tendencies of the NO and AO groups.

Table 1. Summary Statistics of Age Distribution by Group.

Group	Count	Mean	Std	Min	25%	50%	75%	Max
NOs	66.0	16.36	±1.10	14.0	16.0	16.0	17.0	18.0
AOs	65.0	16.90	±0.98	15.0	16.0	17.0	18.0	18.0

All participants were young offenders who received their court orders between 2018 and 2022. These youths were detained for a number of offenses, such as homicide, sexual abuse, theft, violence, illegal possession of weapons/narcotics, and kidnapping (see Figure 3).

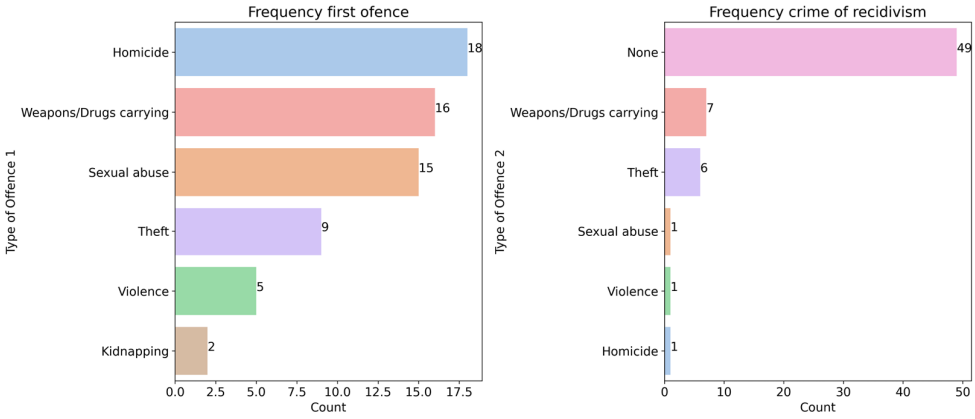

Figure 3. Frequency of the types of crimes committed by offenders, both initially and in cases of recidivism.

The majority of individuals completed up to secondary education, although some only finished primary education. There is a significant number of individuals who have dropped out of the educational system. A significant proportion of these individuals were identified as being associated with gang activities and/or living in a situation of domestic violence. Nevertheless, a significant segment of the study participants had not experienced such situations.

Furthermore, there are individuals who have been displaced due to violence, although they do not constitute the majority of the population under analysis.

Socioeconomic levels 1 and 2 are related to the majority of the population sample from both the offender and non-offender groups. Particularly, out of the 65 people categorized as offenders, 63 belong to socioeconomic level 1 and only 2 belong to level 2. This shows that the lowest socioeconomic level has a significant concentration of offenders. In contrast, among the 66 non-offenders, 22 are in level 1, 43 are in level 2, and 1 is in level 3. This suggests that the non-offender group is more evenly distributed across all socioeconomic groups. It is important to note that the majority (98.5%) of non-offenders still belong to strata 1 and 2.

Between the categories of offenders and non-offenders, there are clear disparities in the analysis of substance use. Comparing offenders to non-offenders, it is clear that the intake of all substances studied, including SPA, alcohol, marijuana, and cocaine, is significantly higher among offenders. Notably, marijuana and cocaine usage are notably common among offenders, while there have been no reports of use among non-offenders (see Figure 4).

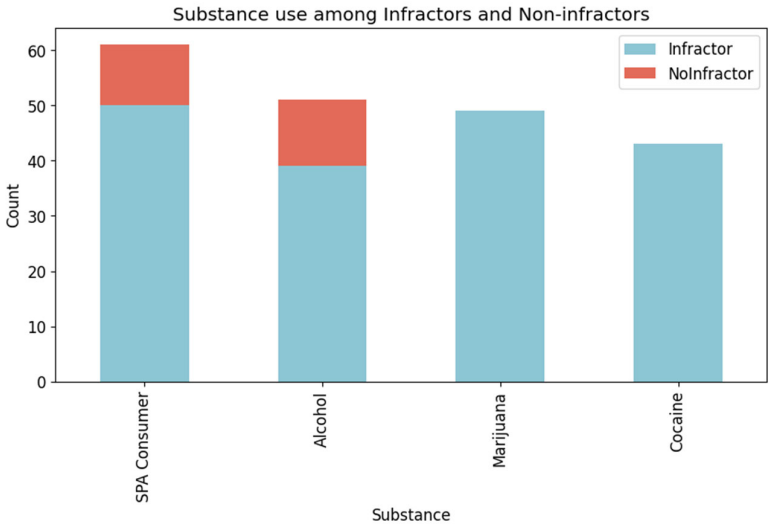

Figure 4. Distribution of SPA, alcohol, marijuana, and cocaine use among offenders and non-offenders.

3.2. Data Processing and Statistical Analysis

3.2.1. Demographic Description

The results of the two-sample *t*-tests are presented in Table 2. There are no significant differences between the two groups in terms of total intracranial volume (TIV), left-cerebral-white-matter volume (left cerebral white matter), and right-cerebral-white-matter volume (right cerebral white matter). However, the average age of AOs is significantly higher than that of NOs (16.91 ± 0.98 vs. 16.36 ± 1.10 years; t = −2.9837; *p*-value < 0.01). Additionally, the left-cerebellum-white-matter volume (left cerebellum white matter) in NOs is significantly larger than in AOs (13,933.47 ± 1448.50 vs. 13,137.88 ± 1279.78; t = 3.3327; *p*-value < 0.01). Similarly, the right-cerebellum-white-matter volume (right cerebellum white matter) in NOs is also significantly larger than in AOs (13,244.94 ± 1467.88 vs. 12,573.94 ± 1348.77; t = 2.7250; *p*-value < 0.01). The interpretation and context of these differences should be considered based on the nature of the study and the specific characteristics of the analyzed groups.

Table 2. Comparison of age and white-matter volumes between the NO and AO groups.

	NOs	AOs	Statistic	*p*-Value
Age	16.36 ± 1.10	16.91 ± 0.98	−2.9837	0.0034
TIV	1,591,143.17 ± 110,783.68	1,558,612.94 ± 135,506.47	1.5030	0.1354
Left cerebral white matter	246,781.85 ± 23,013.65	240,720.29 ± 27,066.44	1.3799	0.1701
Right cerebral white matter	248,298.74 ± 22,578.71	241,914.17 ± 26,878.06	1.4710	0.1438
Left cerebellum white matter	13,933.47 ± 1448.50	13,137.88 ± 1279.78	3.3327	0.0011
Right cerebellum white matter	13,244.94 ± 1467.88	12,573.94 ± 1348.77	2.7250	0.0073

3.2.2. Brain Structural Analysis

The normality assumption in the set of all brain structures of the two groups was evaluated using the Shapiro–Wilk test. Within the control group, it was observed that 88 structures presented data that did not provide sufficient evidence to reject the null hypothesis of normality. However, seven structures displayed statistically significant deviations from normality. In the study group, it was observed that 70 structures exhibited conformity with normality, whereas 25 structures manifested considerable deviations from normality.

Although the Student's *t*-test is robust to non-normality when there is sufficient data, we deemed it statistically appropriate to use non-parametric statistical tests. The Mann–

Whitney test was used to assess differences between the two groups due to its ability to handle non-normal distributions and its suitability for detecting differences in medians (see Table 3).

Table 3. Comparison of Brain Structures using Mann-Whitney U-Statistic and *p*-values.

Brain Structure	U-Statistic	*p*-Value	Cohen's d	Brain Structure	U-Statistic	*p*-Value	Cohen's d
Left cerebellum white matter	2685.0	0.0130	0.423	Ctx-lh-parstriangularis	2886.0	0.0006	0.540
Left thalamus	2650.0	0.0202	0.452	Ctx-lh-posteriorcingulate	2643.0	0.0220	0.468
Left pallidum	2791.0	0.0029	0.525	Ctx-lh-precuneus	2658.0	0.0183	0.449
Brain stem	2816.0	0.0020	0.512	Ctx-lh-rostralmiddlefrontal	3075.0	0.0000	0.851
Left accumbens area	2682.0	0.0135	0.460	Ctx-lh-transversetemporal	2610.0	0.0324	0.396
Left ventral DC	2666.0	0.0165	0.427	Ctx-lh-insula	2637.0	0.0236	0.369
Right lateral ventricle	1640.0	0.0202	−0.364	Ctx-rh-caudalmiddlefrontal	2704.0	0.0101	0.481
Right cerebellum white matter	2618.0	0.0296	0.321	Ctx-rh-entorhinal	2852.0	0.0011	0.469
Right thalamus	2706.0	0.0098	0.457	Ctx-rh-fusiform	2741.0	0.0061	0.478
Right putamen	2621.0	0.0286	0.356	Ctx-rh-inferiortemporal	2724.0	0.0077	0.484
Right pallidum	2802.0	0.0025	0.552	Ctx-rh-isthmuscingulate	2624.0	0.0276	0.374
Right hippocampus	2673.0	0.0151	0.481	Ctx-rh-lateralorbitofrontal	2806.0	0.0023	0.559
Right accumbens area	2814.0	0.0020	0.399	Ctx-rh-lingual	2628.0	0.0263	0.422
Right choroid plexus	1718.0	0.0496	−0.353	Ctx-rh-medialorbitofrontal	2636.0	0.0239	0.430
Ctx-lh-caudalanteriorcingulate	2849.0	0.0012	0.577	Ctx-rh-parahippocampal	2805.0	0.0023	0.557
Ctx-lh-fusiform	2640.0	0.0228	0.341	Ctx-rh-parsorbitalis	2895.0	0.0005	0.618
Ctx-lh-isthmuscingulate	2586.0	0.0425	0.412	Ctx-rh-precuneus	2809.0	0.0022	0.529
ctx-lh-lateralorbitofrontal	2772.0	0.0039	0.527	Ctx-rh-rostralmiddlefrontal	2641.0	0.0225	0.511
Ctx-lh-lingual	2590.0	0.0407	0.321	Ctx-rh-superiorfrontal	2820.0	0.0019	0.586
Ctx-lh-parahippocampal	2778.0	0.0035	0.536	Ctx-rh-superiorparietal	2616.0	0.0303	0.378
Ctx-lh-parsorbitalis	2914.0	0.0004	0.554	Ctx-rh-transversetemporal	2646.0	0.0212	0.418

The results shown that 42 structures have statistically significant dissimilarities between the control and study groups, as evidenced by a p-value < 0.05.

In the left hemisphere, the cerebellum white matter, thalamus, pallidum, brain stem, accumbens area, and ventral DC showed significant differences.

In the right hemisphere, the lateral ventricle, cerebellum white matter, thalamus, putamen, pallidum, hippocampus, and accumbens area exhibited significant differences.

Within the cortical regions of the left hemisphere, the caudal anterior cingulate, fusiform, isthmus cingulate, lateral orbitofrontal, lingual, parahippocampal, pars orbitalis, pars triangularis, posterior cingulate, precuneus, rostral middle frontal, transverse temporal, and insula demonstrated significant deviations.

Similarly, within the cortical regions of the right hemisphere, the caudal middle frontal, entorhinal, fusiform, inferior temporal, isthmus cingulate, lateral orbitofrontal, lingual, medial orbitofrontal, parahippocampal, pars orbitalis, precuneus, rostral middle frontal, superior frontal, superior parietal, and transverse temporal exhibited significant differences.

Regarding the effect size measured using Cohen's d, a notable structure with a pronounced effect size was ctx-lh-rostralmiddlefrontal, which exhibited a value of 0.851. This suggested a substantial difference between the groups. Within the moderate effect size range, most structures, such as the left cerebellum white matter, ctx-lh-parstriangularis, left pallidum, and brain stem, displayed effect sizes between 0.5 and 0.8, indicating these structures as potentially significant due to their evident relevance. Lastly, several structures exhibited subtler effect sizes, suggesting minor differences between the groups. Structures such as the right choroid plexus and right lateral ventricle presented effect sizes within the range of 0.2 to 0.5, which was considered a small to moderate effect (see Figure 5).

Additionally, considering a correlation analysis, the pairs of characteristics with a correlation greater than 80% are the left pallidum and right pallidum, with a correlation of 0.822813, the ctx-rh-precuneus and ctx-lh-precuneus with a correlation of 0.835341, ctx-lh-lateralorbitofrontal and ctx-rh-lateralorbitofrontal with a correlation of 0.843902, the right thalamus and left thalamus with a correlation of 0.913601, and the right cerebellum white matter and left cerebellum white matter with a correlation of 0.927536 (see Figure 6).

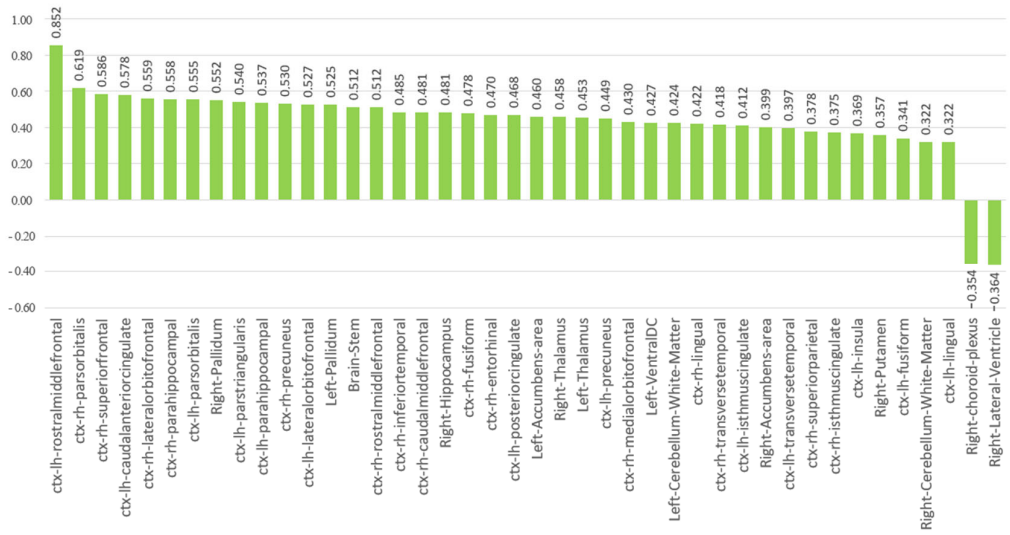

Figure 5. Cohen's d values for each structure with statistically significant differences.

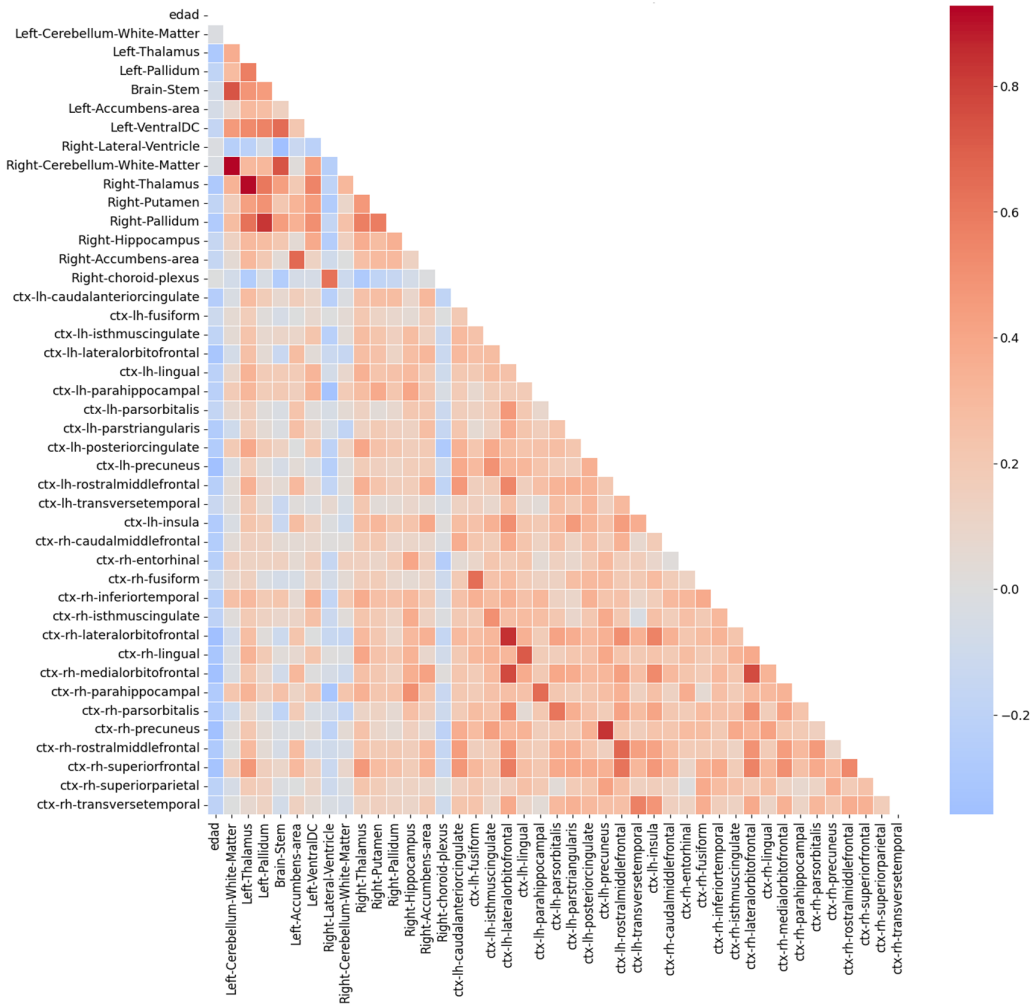

Figure 6. Correlation heat map of brain structures volumes.

3.3. Optimizing Feature Identification through Dimensionality Reduction Techniques

The application of principal component analysis (PCA) was utilized as a method for dimensionality reduction, in order to identify the fundamental characteristics that account for the majority of the variability observed in the data.

The variance attributed to each principal component was assessed, and the cumulative variance explained was computed. The findings indicate that approximately 30 principal components are sufficient to account for 95% of the variance observed in the data (see Figure 7). This implies that it is possible to decrease the dimensionality of the data set, specifically from 43 features to approximately 30 principal components, while retaining a substantial amount of information.

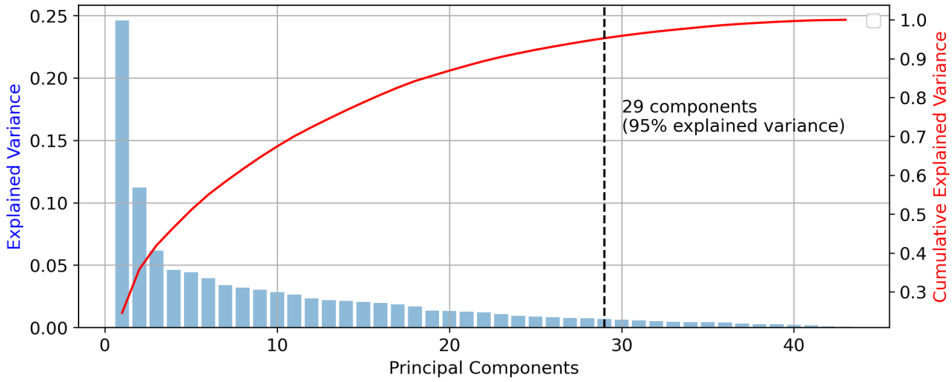

Figure 7. Explained and cumulative variance by principal components in brain structures volumes.

3.4. Optimizing Feature Identification Using Classification Techniques

In order to enhance the efficacy of identifying relevant features, we used the 42 structures that exhibited the highest statistical significance, and 5 distinct classification methods were employed to further refine the detection process. A thorough grid search was performed for each method, in conjunction with cross-validation, to ensure the reliability and applicability of the obtained outcomes. As depicted in Table 4, the DecisionTreeClassifier and RandomForestClassifier exhibited comparable average accuracies of 0.664. The DecisionTreeClassifier attained a maximum accuracy of 0.800 (see Figure 8a), while the RandomForestClassifier achieved a peak accuracy of 0.705. In contrast, the Support Vector Classifier (SVC) exhibited an average accuracy of 0.521, whereas the Gaussian Naive Bayes (GaussianNB) demonstrated comparable performance to the leading classifiers, achieving an average accuracy of 0.663. Finally, the LogisticRegression method yielded an average accuracy of 0.578. Significantly, the GaussianNB classifier achieved the highest maximum accuracy of 0.809 among the classifiers that were tested. Figure 8a shows the behavior of the DecisionTreeClassifier.

Table 4. Accuracy metrics of classification methods for relevant features detection.

Classifier	Average Accuracy	Max Accuracy	Min Accuracy
DecisionTreeClassifier	0.664	0.800	0.571
RandomForestClassifier	0.664	0.705	0.619
SVC	0.521	0.700	0.479
GaussianNB	0.663	0.809	0.571
LogisticRegression	0.578	0.714	0.380

Given that the classifier with the best results is tree-based, the feature importance for classification was then estimated (see Figure 7b). This assessment enables an understanding of which neuroanatomical markers are most influential in determining the classification outcomes. The ctx-lh-rostralmiddlefrontal, left pallidum, and ctx-lh-lingual were the most important structures.

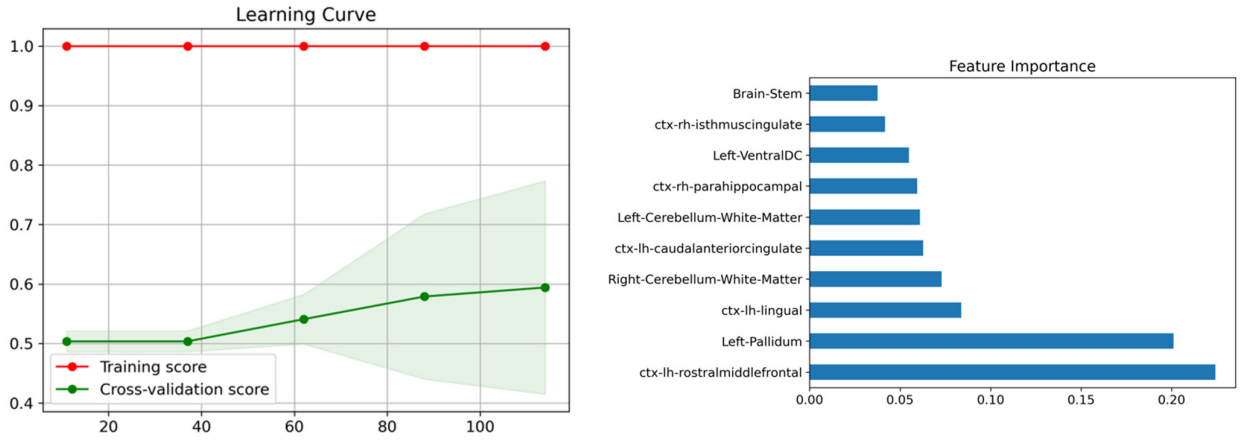

(**a**) (**b**)

Figure 8. Results of (**a**) the decision tree classifier behavior using cross-validation and (**b**) feature importance of the ten most important features.

We investigated the variations in volumes across age within distinct groups. Figure 9 outlines these patterns for the six most important structures. For the ctx-lh-rostralmiddlefrontal structure, the NOs typically exhibit a slightly higher average volume across ages, with the exception of age 17, where the AOs display a significantly lower volume of 0.00788 compared to 0.00913 in the NOs.

The average volume of the left pallidum for the NOs remains relatively constant throughout the ages considered. However, it is noteworthy that, at the age of 18, the AOs possess a notably lower mean volume of 0.00136 compared to the NOs (0.00143). For the ctx-lh-lingual structure, an intriguing behavior is observed. At age 15, the AOs have a higher mean volume of 0.00494 compared to the NOs (0.00477). Yet, at age 16, this trend reverses, with a reduced volume in the AOs of 0.00430 relative to the NOs (0.00458). At age 17, the AOs once again display a slightly elevated volume.

In the right cerebellum white matter, the NOs generally possess a higher average volume throughout the ages studied when compared to the AOs, except at age 17, where both groups showcase very similar volumes. For the ctx-lh-caudalanteriorcingulate structure, at age 15, the AOs have a lower average volume of 0.00250 in comparison to the NOs (0.00266). However, at age 16, the AOs exhibit an increase, surpassing the NOs with a volume of 0.00260 against 0.00251. At subsequent ages, the NOs tend to exhibit a slightly higher mean volume relative to the AOs. For the left cerebellum white matter, the NOs consistently have higher average volumes across the ages when compared to the AOs, although the differences are not as pronounced.

The analysis of the observations indicates an unclear pattern in the increase or decrease in brain volume in relation to age across the examined structures and groups (see Figure 10). It is imperative to recognize the potential for the sample to lack complete representativeness, as well as the existence of confounding variables that have not yet been accounted for in this study.

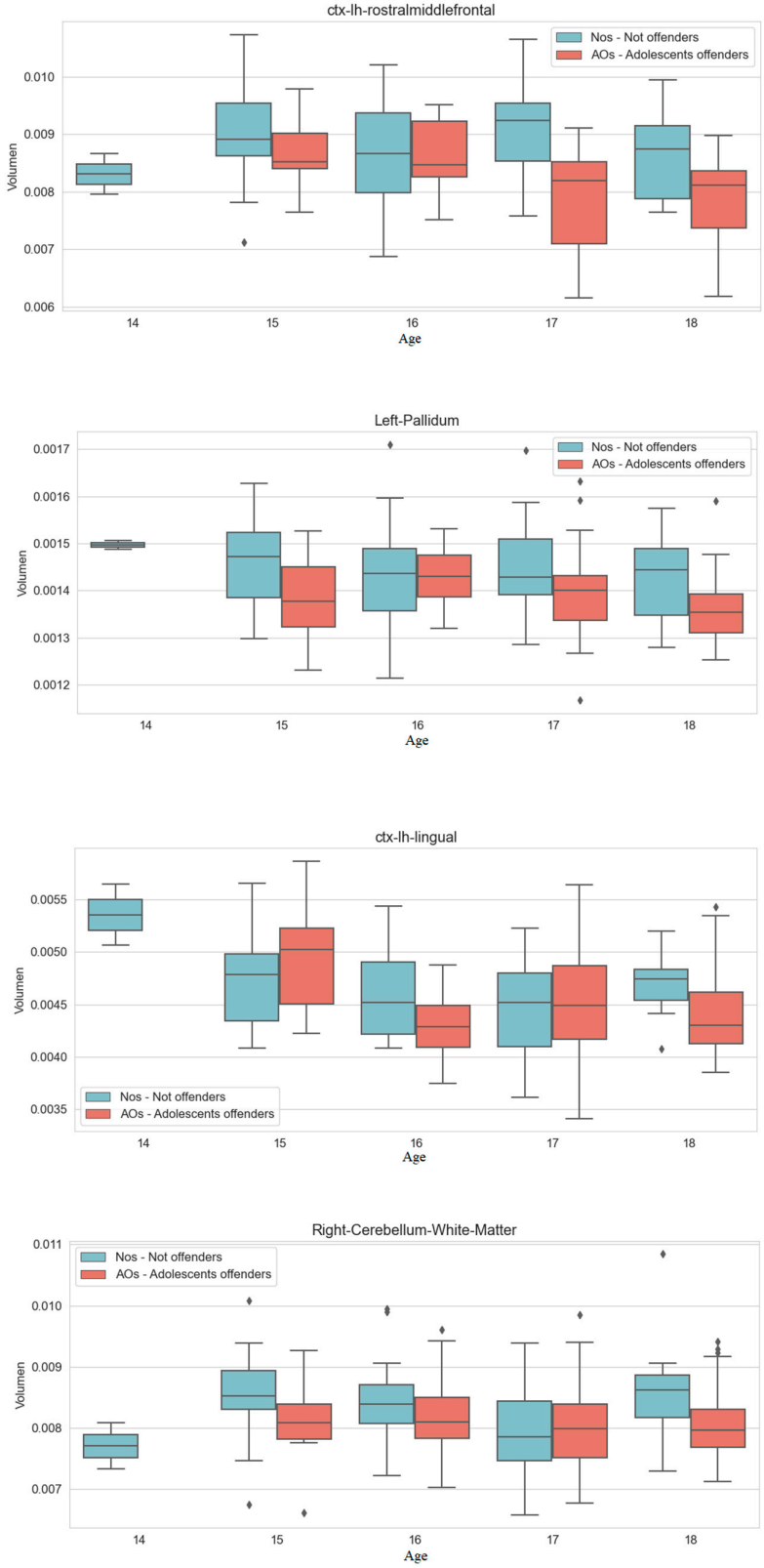

Figure 9. *Cont.*

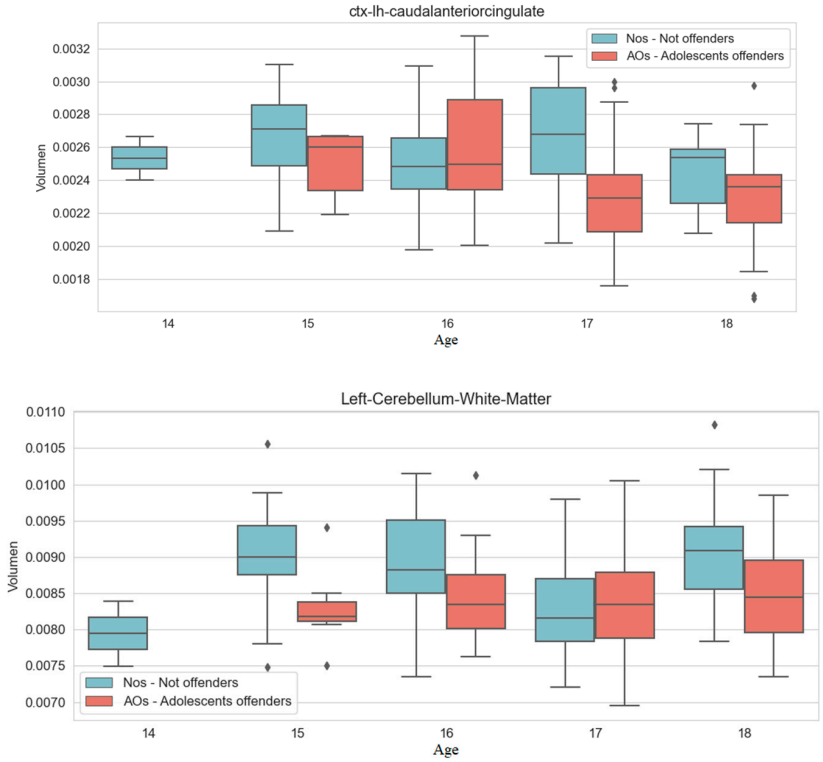

Figure 9. Comparative volumetric analysis of selected brain structures between not offenders and adolescent offenders across different ages.

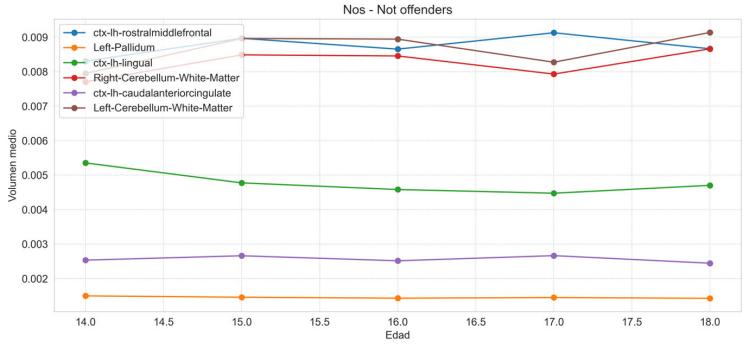

(**a**)

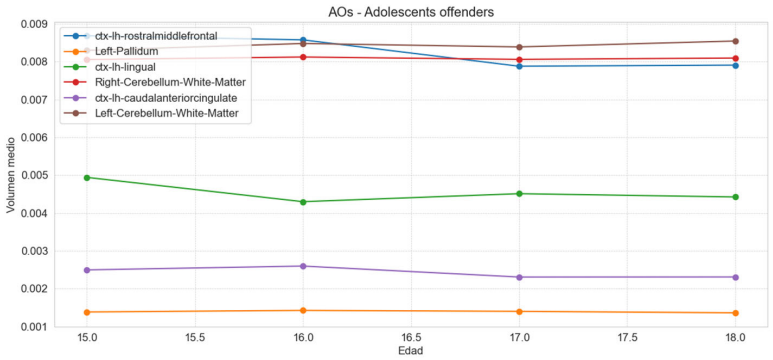

(**b**)

Figure 10. Comparative analysis of average brain structure volumes across ages for (**a**) not offenders, and (**b**) adolescent offenders.

4. Discussion

4.1. Demographic and Behavioral Analysis

Our primary intent was to discern the neuroanatomical disparities between adolescent offenders (AOs) and non-offenders (NOs). The outcomes of the two-sample *t*-tests manifest that while there are no significant disparities between the groups concerning total intracranial volume (TIV) and cerebral white-matter volumes, there are differences in age and cerebellar-white-matter volumes.

The statistically significant age difference between the groups, with the AOs being older on average, could potentially introduce biases in the analysis. Older adolescents might naturally exhibit certain neuroanatomical variations due to the ongoing maturation processes during this period. This age variance raises an essential question related to whether observed structural differences could be attributable to the age-related maturation of specific brain regions rather than being inherent characteristics of the offender group. However, the absence of significant differences in TIV between the groups somewhat mitigates this concern. The consistent TIV across groups suggests that, despite potential age-related differences, the overall intracranial volumes remain invariant between the two populations.

While cerebral-white-matter volumes show no significant disparity, a marked difference in cerebellar-white-matter volumes between the groups was found. Specifically, the NOs exhibit significantly greater volumes of cerebellar white matter, both on the left and right sides, compared to the AOs. The cerebellum, traditionally associated with motor functions, has more recently been implicated in cognitive and emotional processing. Given its diverse roles, a reduced white-matter volume in the cerebellum of AOs could potentially be associated with functional implications, from motor coordination to emotional regulation.

4.2. Socioeconomic and Substance Use Analysis

Socioeconomic considerations were prominently highlighted in our analysis. The data displayed a pronounced skew in the offender group towards the lower socioeconomic tiers. The majority (96.9%) of the AOs originated from socioeconomic level 1. This stark distinction, in comparison to the NOs who showcased a more balanced distribution across socioeconomic tiers, accentuates the potential influence of socioeconomic conditions on delinquent propensities. Notwithstanding, it is of significance to observe that a considerable majority (98.5%) of the NOs predominantly lean towards the lower socioeconomic tiers (levels 1 and 2).

A discrepancy was observed between the AOs and NOs, with the former demonstrating markedly elevated substance consumption. In particular, the incidence of marijuana and cocaine usage among the AOs was considerably elevated, emphasizing the potential ramifications of substance misuse on adolescent delinquency.

The intricate relationship between substance use and neuroanatomical variations presents a complex challenge. A pivotal question arises: Is substance use a consequence of inherent anatomical brain characteristics, or does substance consumption drive the observed alterations in brain structure volumes? It becomes essential to consider the bidirectional nature of this relationship. Disentangling these intertwined factors necessitates longitudinal studies, with repeated neuroimaging and substance use assessments, to elucidate the causal pathways and temporal dynamics underpinning these associations.

4.3. Neuroanatomical Insights

The brain structures that exhibited significant differences between AOs and NOs encompass the frontal lobe (ctx-lh-rostralmiddlefrontal), the left pallidum (left pallidum), the occipital lobe (ctx-lh-lingual), and the cerebellum (right cerebellum white matter and left cerebellum white matter), as well as another region in the frontal lobe (ctx-lh-caudalanteriorcingulate). Table 5 provides their descriptions and specific locations in the brain. Table 6 presents their associated behavioral functions, and potential links to violent behavior.

Table 5. Brain structures, their descriptions, and locations in the brain.

Structure	Description	Location
Ctx-lh-rostralmiddlefrontal	A portion of the left frontal cortex in the brain's left hemisphere.	Frontal lobe, left hemisphere.
Left pallidum	The subcortical component of the basal ganglia.	Base of the brain, left hemisphere.
Ctx-lh-lingual	A brain gyrus found between the calcarine sulcus and the collateral sulcus.	Occipital lobe, left hemisphere.
Right cerebellum white matter Left cerebellum white matter	The portion of the cerebellum's white matter containing nerve fibers that connect the cerebellum to other brain regions and the spinal cord.	Cerebellum, right and left hemisphere.
ctx-lh-caudalanteriorcingulate	Frontal and apical portion of the cingulate cortex, located in the corpus callosum.	Frontal lobe, near the corpus callosum, left hemisphere.

The involvement of the frontal lobe, specifically the ctx-lh-rostralmiddlefrontal and ctx-lh-caudalanteriorcingulate regions, aligns with prior research indicating that this area is intrinsically linked with behavioral regulation, decision-making, and the inhibition of impulsive responses [40,41]. A diminished or altered volume in these regions might correlate with a propensity for violent or impulsive behaviors. Notably, the rostral middle frontal cortex is associated with executive functions, while the caudal anterior cingulate cortex plays a role in conflict detection and emotional regulation.

The left pallidum is a component of the basal ganglia system and is engaged in the regulation of voluntary movements. While not typically directly associated with violent behavior, any anomaly in this region might hint at broader discrepancies in brain structure and function. However, the findings on the pallidum align with findings in [42]. There is a reduced volume in the right pallidum for Pediatric Bipolar Disorder patients. A strong link was found between the number of episodes and the connectivity between the left pallidum and right caudate. The Pediatric Bipolar Disorder group also showed disrupted brain connectivity compared to healthy individuals. Some works also study its relationship with schizophrenia [43].

The occipital lobe, particularly the ctx-lh-lingual region, primarily manages visual processing. Differences in this area might suggest variations in visual perception or processing between AOs and NOs, although the direct link with criminal behavior remains uncertain and may be indirect.

The cerebellum, as represented by the right-cerebellum-white-matter and left-cerebellum-white-matter areas, has traditionally been viewed as a coordinator of motor functions. Yet, recent studies suggest it might also be implicated in cognitive and emotional functions [44]. Anomalies in the cerebellum's white-matter volume could indicate differences in neural connectivity and information integration.

4.4. Data Processing and Machine Learning Insights

The study's comprehensive data processing and statistical analysis supported the validity of the results. The application of machine learning, notably dimensionality reduction techniques, provided valuable insights. Through principal component analysis (PCA), data dimensions were reduced while preserving most of the variance, as evidenced by approximately 30 principal components accounting for 95% of the cumulative data variance.

The exploration of classification techniques aimed at optimizing feature identification was also undertaken. Five classification methods were utilized, with the DecisionTreeClassifier and RandomForestClassifier identified as having the highest accuracy. The feature importance derived from these classifiers highlighted the relevance of structures such as the ctx-lh-rostralmiddlefrontal, left pallidum, and ctx-lh-lingual in differentiating between the groups.

4.5. Limitations and Concluding Remarks

While our study offers promising insights, it is not devoid of limitations. The potential for the sample to lack full representativeness looms large, and other confounding variables not considered could influence the results. The intricate interplay of neuroanatomical differences, socioeconomic conditions, substance abuse, and genetic and environmental factors poses intriguing questions for future research. Our findings, while pivotal, represent just one facet of a complex puzzle, and further studies are essential to decode the myriad influences on adolescent criminal behavior.

Table 6. Brain structures, their behavioral functions, and associations with violent behavior.

Structure	Function Related to Behavior	Relation to Violent Behavior
Frontal Lobe (ctx-lh-rostralmiddlefrontal)	Involved in cognitive processes of a higher nature, such as the faculties of reasoning, planning, decision-making, and impulse control [45]. Additionally, it is implicated in the regulation of emotions and the development of personality traits.	Lesions or dysfunctions within this particular region have been observed to potentially correlate with impulsivity, deficiency in empathy, and the manifestation of aggressive behavior [46–48].
Left Globus Pallidus (left pallidum)	The primary function of the globus pallidus is to control conscious and proprioceptive movements [49].	Although its dysfunction is not directly related to violent behavior, it can affect motor regulation and certain cognitive aspects [50].
Occipital Lobe (ctx-lh-lingual)	Primarily concerned with visual processing, particularly word and object recognition [51–53].	No direct relationship established with violent behavior [54].
Cerebellum (right cerebellum white matter and left cerebellum white matter)	Traditionally associated with motor coordination, but studies suggests a role in cognitive and emotional functions [44,55,56].	Alterations in the cerebellum may be related to autism spectrum disorders and schizophrenia, but no direct relationship established with violent behavior [44].
Frontal Lobe (ctx-lh-caudalanteriorcingulate)	Involved in emotional regulation, decision-making, and reward anticipation. Also plays a role in motor and cognitive control [45].	Dysfunctions in this region may be related to anxiety disorders, depression, and ADHD. There may be an indirect relationship with impulsive behaviors [57,58].

5. Conclusions

Distinct neuroanatomical disparities have been identified between adolescent offenders (AOs) and non-offenders (NOs). While there was no significant difference in total intracranial volume (TIV) between the two groups, offering a consistent basis for comparisons, differences in cerebellar-white-matter volumes were evident. Specifically, non-offenders exhibited significantly larger volumes on both sides, with a substantial effect size represented by a Cohen's d of 0.82 for the left side and 0.78 for the right side. These differences suggest potential functional implications, which could range from motor coordination to emotional regulation.

A clear distinction in socioeconomic backgrounds and substance use patterns was observed. The skew of AOs towards the lower socioeconomic tiers, coupled with their elevated substance consumption, especially marijuana and cocaine, could accentuate the potential impact of these factors on adolescent behavior.

In terms of specific brain regions, the frontal lobe, left pallidum, occipital lobe, and cerebellum presented notable volume variations between the two groups. Such variations might offer insights into behavioral tendencies, especially considering that regions like the rostral middle frontal cortex and caudal anterior cingulate cortex have intrinsic associations with behavior regulation and emotional control.

This study not only employed traditional statistical analyses but also delved deeply into machine learning techniques to reinforce the findings. The application of machine learning, especially principal component analysis, recursive feature elimination, and classi-

fication techniques, provided a richer perspective of the data, highlighting the relevance of various brain structures in differentiating between the two groups.

However, the sample size used for this study may be a limiting factor in the generalizability of the results. It underscores the importance of further work with larger and more diverse samples to validate and expand upon these findings.

Author Contributions: Conceptualization, G.S.-T., M.P. and N.L.; methodology, G.S.-T. and N.L.; software, G.S.-T. and N.L.; validation, N.L., M.P. and G.S.-T.; investigation, G.S.-T., N.L. and M.P.; data curation, G.S.-T. and N.L.; writing—original draft preparation, G.S.-T.; writing—review and editing, N.L. and M.P.; visualization, G.S.-T.; supervision, M.P.; funding acquisition, M.P. All authors have read and agreed to the published version of the manuscript.

Funding: This research and APC was funded by Ministerio de Ciencia Tecnología e Innovación in Colombia, grant number 68229 BPIN 20200000100006.

Institutional Review Board Statement: The study was conducted in accordance with the Declaration of Helsinki and was approved by the Ethics Committee of Universidad del Magdalena, in line with national regulation Res. 8430 de 1993 from the Ministry of Health, on 23 May 2019.

Informed Consent Statement: Informed consent was obtained from all subjects involved in the study.

Data Availability Statement: The data presented in this study are openly available in Zenodo at https://zenodo.org/record/8310407, DOI 10.5281/zenodo.8310407.

Acknowledgments: We would like to extend our gratitude for the support received from Ministerio de Ciencia Tecnología e Innovación—MinCiencias Colombia, and the *Fundación Clarets*, the *Centro de Reeducación el Oasis, and the Fundación Luz Esperanza* in Barranquilla, Colombia, their invaluable contributions significantly facilitated the realization of this research.

Conflicts of Interest: The authors declare no conflicts of interest.

References

1. Amri, M.M.; Abed, S.A. The Data-Driven Future of Healthcare: A Review. *Mesopotamian J. Big Data* **2023**, *2023*, 68–74. [CrossRef]
2. Ling, S.; Umbach, R.; Raine, A. Biological Explanations of Criminal Behavior. *Psychol. Crime. Law PC L* **2019**, *25*, 626–640. [CrossRef] [PubMed]
3. Miller, E. Brain Injury as a Contributory Factor in Offending. In *The Neurobiology of Criminal Behavior*; Glicksohn, J., Ed.; Neurobiological Foundation of Aberrant Behaviors; Springer: Boston, MA, USA, 2002; pp. 137–153, ISBN 978-1-4615-0943-1.
4. Hofhansel, L.; Weidler, C.; Votinov, M.; Clemens, B.; Raine, A.; Habel, U. Morphology of the Criminal Brain: Gray Matter Reductions Are Linked to Antisocial Behavior in Offenders. *Brain Struct. Funct.* **2020**, *225*, 2017–2028. [CrossRef] [PubMed]
5. Loomans, M.M.; Tulen, J.H.M.; van Marle, H.J.C. The neurobiology of antisocial behaviour. *Tijdschr. Voor Psychiatr.* **2010**, *52*, 387–396.
6. Liu, H.; Li, Y.; Guo, G. Gene by Social-Environment Interaction for Youth Delinquency and Violence: Thirty-Nine Aggression-Related Genes. *Soc. Forces Sci. Medium Soc. Study Interpret.* **2015**, *93*, 881–903. [CrossRef]
7. Reiss, D.; Ganiban, J.M.; Leve, L.D.; Neiderhiser, J.M.; Shaw, D.S.; Natsuaki, M.N. Parenting in the Context of the Child: Genetic and Social Processes. *Monogr. Soc. Res. Child Dev.* **2022**, *87*, 7–188. [CrossRef]
8. Jones, M.S.; Hoffmann, J.P. Measuring Adverse Childhood Experiences with Latent Class Trajectories. *Child Abus. Negl.* **2023**, *140*, 106142. [CrossRef]
9. Morgan, P.L.; Farkas, G.; Woods, A.D.; Wang, Y.; Hillemeier, M.M.; Oh, Y. Factors Predictive of Being Bullies or Victims of Bullies in US Elementary Schools. *Sch. Ment. Health* **2023**, *15*, 566–582. [CrossRef]
10. Turner, D.; Wolf, A.J.; Barra, S.; Müller, M.; Gregório Hertz, P.; Huss, M.; Tüscher, O.; Retz, W. The Association between Adverse Childhood Experiences and Mental Health Problems in Young Offenders. *Eur. Child Adolesc. Psychiatry* **2021**, *30*, 1195–1207. [CrossRef]
11. Perino, M.T.; Guassi Moreira, J.F.; Telzer, E.H. Links between Adolescent Bullying and Neural Activation to Viewing Social Exclusion. *Cogn. Affect. Behav. Neurosci.* **2019**, *19*, 1467–1478. [CrossRef]
12. Geurts, D.E.M.; von Borries, K.; Huys, Q.J.M.; Bulten, B.H.; Verkes, R.-J.; Cools, R. Psychopathic Tendency in Violent Offenders Is Associated with Reduced Aversive Pavlovian Inhibition of Behavior and Associated Striatal BOLD Signal. *Front. Behav. Neurosci.* **2022**, *16*, 963776. [CrossRef] [PubMed]
13. Pino, M.; Montaño, S.; Agudelo, K.; Idárraga-Cabrera, C.; Fernández-Lucas, J.; Herrera-Mendoza, K. Emotion Recognition in Young Male Offenders and Non-Offenders. *Physiol. Behav.* **2019**, *207*, 73–75. [CrossRef] [PubMed]
14. Llorca Mestre, A.; Malonda, E.; Samper-García, P. Depression and Aggressive Behaviour in Adolescents Offenders and Non-Offenders. *Psicothema* **2017**, *29*, 197–203. [CrossRef] [PubMed]

15. Olivera-La Rosa, A.; Amador, O.; Chuquichambi, E.G.; Carmona-Cardona, C.A.; Acosta-Tobón, S.A.; Arango-Tobón, O.E.; Villacampa, J. Exploring the Relationship between Callous-Unemotional Traits and Implicit Attitudes toward Violence. *Healthcare* **2023**, *11*, 1445. [CrossRef] [PubMed]
16. Navarro-Pérez, J.-J.; Viera, M.; Calero, J.; Tomás, J.M. Factors in Assessing Recidivism Risk in Young Offenders. *Sustainability* **2020**, *12*, 1111. [CrossRef]
17. Galinari, L.S.; Bazon, M.R. Criminal Behavior and Psychosocial Risk Factors in Brazilian Adolescent Offenders: An Exploratory Latent Class Analysis. *Int. J. Environ. Res. Public. Health* **2021**, *18*, 10509. [CrossRef]
18. Ritchie, K.; Ancelin, M.L.; Amieva, H.; Rouaud, O.; Carrière, I. The Association between Caffeine and Cognitive Decline: Examining Alternative Causal Hypotheses. *Int. Psychogeriatr.* **2014**, *26*, 581–590. [CrossRef]
19. Gross, J.J.; Thompson, R.A. Emotion Regulation: Conceptual Foundations. In *Handbook of Emotion Regulation*; The Guilford Press: New York, NY, USA, 2007; pp. 3–24, ISBN 978-1-59385-148-4.
20. Paulus, F.W.; Ohmann, S.; Möhler, E.; Plener, P.; Popow, C. Emotional Dysregulation in Children and Adolescents With Psychiatric Disorders. A Narrative Review. *Front. Psychiatry* **2021**, *12*, 628252. [CrossRef]
21. Njardvik, U.; Smaradottir, H.; Öst, L.-G. The Effects of Emotion Regulation Treatment on Disruptive Behavior Problems in Children: A Randomized Controlled Trial. *Res. Child Adolesc. Psychopathol.* **2022**, *50*, 895–905. [CrossRef]
22. McLaughlin, K.A.; Hatzenbuehler, M.L.; Mennin, D.S.; Nolen-Hoeksema, S. Emotion Dysregulation and Adolescent Psychopathology: A Prospective Study. *Behav. Res. Ther.* **2011**, *49*, 544–554. [CrossRef]
23. Gross, J.J. Emotion Regulation: Current Status and Future Prospects. *Psychol. Inq.* **2015**, *26*, 1–26. [CrossRef]
24. Salinas, K.Z.; Venta, A. Testing the Role of Emotion Dysregulation as a Predictor of Juvenile Recidivism. *Eur. J. Investig. Health Psychol. Educ.* **2021**, *11*, 83–95. [CrossRef] [PubMed]
25. Roberton, T.; Daffern, M.; Bucks, R.S. Emotion Regulation and Aggression. *Aggress. Violent Behav.* **2012**, *17*, 72–82. [CrossRef]
26. Kemp, K.; Thamotharan, S.; Poindexter, B.; Barker, D.; Tolou-Shams, M.; Houck, C.D. Emotion regulation as a predictor of juvenile arrest. *Crim. Justice Behav.* **2017**, *44*, 912–926. [CrossRef] [PubMed]
27. Habersaat, S.; Urben, S. Anger Dysregulation in Adolescents with Persisting Offending Behaviors. In *Anger and Anxiety: Predictors, Coping Strategies, and Health Effects*; Psychology of Emotions, Motivations and Actions; Nova Science Publishers: Hauppauge, NY, USA, 2017; pp. 107–133. ISBN 978-1-5361-2931-1.
28. Yousaf, T.; Dervenoulas, G.; Politis, M. Advances in MRI Methodology. *Int. Rev. Neurobiol.* **2018**, *141*, 31–76. [CrossRef] [PubMed]
29. Oostermeijer, S.; Whittle, S.; Suo, C.; Allen, N.B.; Simmons, J.G.; Vijayakumar, N.; van de Ven, P.M.; Jansen, L.M.C.; Yücel, M.; Popma, A. Trajectories of Adolescent Conduct Problems in Relation to Cortical Thickness Development: A Longitudinal MRI Study. *Transl. Psychiatry* **2016**, *6*, e841. [CrossRef] [PubMed]
30. Miskovich, T.A.; Anderson, N.E.; Harenski, C.L.; Harenski, K.A.; Baskin-Sommers, A.R.; Larson, C.L.; Newman, J.P.; Hanson, J.L.; Stout, D.M.; Koenigs, M.; et al. Abnormal Cortical Gyrification in Criminal Psychopathy. *NeuroImage Clin.* **2018**, *19*, 876–882. [CrossRef] [PubMed]
31. Besteher, B.; Squarcina, L.; Spalthoff, R.; Bellani, M.; Gaser, C.; Brambilla, P.; Nenadić, I. Brain Structural Correlates of Irritability: Findings in a Large Healthy Cohort. *Hum. Brain Mapp.* **2017**, *38*, 6230–6238. [CrossRef]
32. Yang, Y.; Raine, A. Prefrontal Structural and Functional Brain Imaging Findings in Antisocial, Violent, and Psychopathic Individuals: A Meta-Analysis. *Psychiatry Res.* **2009**, *174*, 81–88. [CrossRef]
33. Liu, W.; Wang, J. Recursive Elimination–Election Algorithms for Wrapper Feature Selection. *Appl. Soft Comput.* **2021**, *113*, 107956. [CrossRef]
34. Tibshirani, R. Regression Shrinkage and Selection via the Lasso. *J. R. Stat. Soc. Ser. B Methodol.* **1996**, *58*, 267–288. [CrossRef]
35. Fischl, B. FreeSurfer. *Neuroimage* **2012**, *62*, 774–781. [CrossRef] [PubMed]
36. Belaroussi, B.; Milles, J.; Carme, S.; Zhu, Y.M.; Benoit-Cattin, H. Intensity Non-Uniformity Correction in MRI: Existing Methods and Their Validation. *Med. Image Anal.* **2006**, *10*, 234–246. [CrossRef] [PubMed]
37. Vovk, U.; Pernus, F.; Likar, B. A Review of Methods for Correction of Intensity Inhomogeneity in MRI. *IEEE Trans. Med. Imaging* **2007**, *26*, 405–421. [CrossRef]
38. Nowinski, W.L.; Qian, G.; Bhanu Prakash, K.N.; Hu, Q.; Aziz, A. Fast Talairach Transformation for Magnetic Resonance Neuroimages. *J. Comput. Assist. Tomogr.* **2006**, *30*, 629–641. [CrossRef] [PubMed]
39. Arce-Santana, E.; Campos-Delgado, D.U.; Reducindo, I.; Mejía-Rodríguez, A.R.; Rizzo, G. Rigid Multimodal/Multispectral Image Registration Based on the Expectation-Maximization Algorithm. In *Advances in Visual Computing: 10th International Symposium, ISVC 2014, Las Vegas, NV, USA, 8–10 December 2014*; Bebis, G., Boyle, R., Parvin, B., Koracin, D., McMahan, R., Jerald, J., Zhang, H., Drucker, S.M., Kambhamettu, C., El Choubassi, M., et al., Eds.; Springer International Publishing: Cham, Switzerland, 2014; pp. 11–20.
40. Gavazzi, G.; Giovannelli, F.; Noferini, C.; Cincotta, M.; Cavaliere, C.; Salvatore, M.; Mascalchi, M.; Viggiano, M.P. Subregional Prefrontal Cortex Recruitment as a Function of Inhibitory Demand: An fMRI Metanalysis. *Neurosci. Biobehav. Rev.* **2023**, *152*, 105285. [CrossRef] [PubMed]
41. Pirau, L.; Lui, F. Frontal Lobe Syndrome. In *StatPearls*; StatPearls Publishing: Treasure Island, FL, USA, 2023.
42. Zhang, X.; Gao, W.; Cao, W.; Kuang, L.; Niu, J.; Guo, Y.; Cui, D.; Jiao, Q.; Qiu, J.; Su, L.; et al. Pallidal Volume Reduction and Prefrontal-Striatal-Thalamic Functional Connectivity Disruption in Pediatric Bipolar Disorders. *J. Affect. Disord.* **2022**, *301*, 281–288. [CrossRef]

43. Qi, W.; Wen, Z.; Chen, J.; Capichioni, G.; Ando, F.; Chen, Z.S.; Wang, J.; Yoncheva, Y.; Castellanos, F.X.; Milad, M.; et al. Aberrant Resting-State Functional Connectivity of the Globus Pallidus Interna in First-Episode Schizophrenia. *Schizophr. Res.* **2023**, *261*, 100–106. [CrossRef]
44. Baumann, O.; Mattingley, J.B. Cerebellum and Emotion Processing. *Adv. Exp. Med. Biol.* **2022**, *1378*, 25–39. [CrossRef]
45. Catani, M. The Anatomy of the Human Frontal Lobe. *Handb. Clin. Neurol.* **2019**, *163*, 95–122. [CrossRef]
46. Valdés, G.J.L.; Torrealba, L.F. La Corteza Prefrontal Medial Controla El Alerta Conductual y Vegetativo: Implicancias En Desórdenes de La Conducta. *Rev. Chil. Neuro-Psiquiatr.* **2006**, *44*, 195–204. [CrossRef]
47. Gilbert, S.J.; Williamson, I.D.M.; Dumontheil, I.; Simons, J.S.; Frith, C.D.; Burgess, P.W. Distinct Regions of Medial Rostral Prefrontal Cortex Supporting Social and Nonsocial Functions. *Soc. Cogn. Affect. Neurosci.* **2007**, *2*, 217–226. [CrossRef] [PubMed]
48. Dumontheil, I.; Burgess, P.W.; Blakemore, S.-J. Development of Rostral Prefrontal Cortex and Cognitive and Behavioural Disorders. *Dev. Med. Child Neurol.* **2008**, *50*, 168–181. [CrossRef] [PubMed]
49. Javed, N.; Cascella, M. Neuroanatomy, Globus Pallidus. In *StatPearls*; StatPearls Publishing: Treasure Island, FL, USA, 2023.
50. Gu, B.-M.; Schmidt, R.; Berke, J.D. Globus Pallidus Dynamics Reveal Covert Strategies for Behavioral Inhibition. *eLife* **2020**, *9*, e57215. [CrossRef] [PubMed]
51. Lingnau, A.; Downing, P.E. The Lateral Occipitotemporal Cortex in Action. *Trends Cogn. Sci.* **2015**, *19*, 268–277. [CrossRef] [PubMed]
52. Hannagan, T.; Amedi, A.; Cohen, L.; Dehaene-Lambertz, G.; Dehaene, S. Origins of the Specialization for Letters and Numbers in Ventral Occipitotemporal Cortex. *Trends Cogn. Sci.* **2015**, *19*, 374–382. [CrossRef] [PubMed]
53. Zhang, B.; He, S.; Weng, X. Localization and Functional Characterization of an Occipital Visual Word Form Sensitive Area. *Sci. Rep.* **2018**, *8*, 6723. [CrossRef] [PubMed]
54. Palejwala, A.H.; Dadario, N.B.; Young, I.M.; O'Connor, K.; Briggs, R.G.; Conner, A.K.; O'Donoghue, D.L.; Sughrue, M.E. Anatomy and White Matter Connections of the Lingual Gyrus and Cuneus. *World Neurosurg.* **2021**, *151*, e426–e437. [CrossRef]
55. Adamaszek, M.; D'Agata, F.; Ferrucci, R.; Habas, C.; Keulen, S.; Kirkby, K.C.; Leggio, M.; Mariën, P.; Molinari, M.; Moulton, E.; et al. Consensus Paper: Cerebellum and Emotion. *Cerebellum Lond. Engl.* **2017**, *16*, 552–576. [CrossRef]
56. Pierce, J.E.; Péron, J. The Basal Ganglia and the Cerebellum in Human Emotion. *Soc. Cogn. Affect. Neurosci.* **2020**, *15*, 599–613. [CrossRef]
57. Boes, A.D.; Tranel, D.; Anderson, S.W.; Nopoulos, P. Right Anterior Cingulate: A Neuroanatomical Correlate of Aggression and Defiance in Boys. *Behav. Neurosci.* **2008**, *122*, 677–684. [CrossRef] [PubMed]
58. Taubner, S.; Hauschild, S.; Wisniewski, D.; Wolter, S.; Roth, G.; Fehr, T. Neural Response to Aggressive and Positive Interactions in Violent Offenders and Nonviolent Individuals. *Brain Behav.* **2021**, *11*, e32400. [CrossRef] [PubMed]